

A Supervised Molecular Dynamics Approach to Unbiased Ligand-Protein Unbinding

Giuseppe Degnatti[§], Stefano Moro[#], and Christopher A. Reynolds[§].*

**author to whom correspondence should be addressed: gd17863@essex.ac.uk*

[§] School of Life Sciences, University of Essex, Wivenhoe Park, Colchester, CO4 3SQ, U.K

[#] Molecular Modeling Section, Department of Pharmaceutical and Pharmacological Sciences, University of Padova, Via Marzolo 5, 35131, Padova, Italy

KEYWORDS

Ligand unbinding; binding kinetics; molecular dynamics; supervised molecular dynamics; G protein-coupled receptors; adenosine receptors; muscarinic receptors, orexin receptors; soluble epoxide hydrolase

ABSTRACT

The recent paradigm shift towards the use of the kinetics parameters in place of thermodynamic constants is leading the computational chemistry community to develop methods for studying the mechanisms of drug binding and unbinding. From this standpoint, molecular dynamics (MD) plays an important role, in delivering insight at the molecular scale. However, a known limitation of MD is that the time scales are usually far from those involved in ligand-receptor unbinding events.

Here we show that the algorithm behind supervised MD (SuMD) can simulate the dissociation mechanism of drug-like small molecules while avoiding the input of any energy bias to facilitate the transition. SuMD was tested on seven different intermolecular complexes, covering four G protein-coupled receptors (GPCRs): the A_{2A} and A₁ adenosine receptors, the orexin 2 and the muscarinic 2 receptors, and the soluble globular enzyme epoxide hydrolase. SuMD well-described the multistep nature of ligand-receptor dissociation, rationalized previous experimental data and produced valuable working hypotheses for structure-kinetics relationships (SKR).

INTRODUCTION

Living organisms are open systems and are therefore characterized by absorption, distribution, metabolism and elimination (ADME) phenomena. It follows that the tissue concentration of drugs in proximity to their biological targets is subject to continual variations that do not always justify the use of thermodynamics binding constants (i.e. the dissociation constant K_D - is measured in non-physiological, steady-state conditions) to quantify activities, and drive further drug developments. In this scenario, the concept of binding kinetics is gaining importance¹⁻³, as the dynamic aspect of chemical equilibria relates the K_D with the kinetics constants of formation (k_{on}) and dissociation (k_{off}) for any noncovalent intermolecular complex:

$$K_D = \frac{k_{off}}{k_{on}} \quad (1)$$

Notably, while the drug-receptor binding has a stochastic component that relies on the ligand concentration (influences the ligand probability to be in the proximity of the target), the dissociation is driven only by the free energy required to break the interactions with the receptor, trigger conformational changes, or re-solvate the system. Recently, the residence time (RT - the

reciprocal of the kinetic unbinding constant k_{off}) has been successfully employed in drug discovery campaigns, as can well correlate with drugs activity⁴⁻⁷. However, in spite of the scientific community's efforts in developing robust structure-kinetic relationships (SKRs)¹, the success in using kinetics parameters has been so far limited by the high degree of system-dependency. Indeed, medicinal chemistry strategies to tune the kinetics of a chemical series on one particular biological target may be unsuccessful when applied to a different scaffold, even if it binds in a similar fashion. Any attempt to improve a SKR should be robustly rooted in the mechanistic model of the association/dissociation events implicated and given that X-ray and cryo-EM determinations usually deliver insight only from thermodynamically stable complexes, it follows that computational (un)binding pathways will become increasingly important.

Molecular dynamics (MD) represents a state-of-the-art computational tool routinely employed for structure-based drug design (SBDD). MD describes the time evolution of biomolecular systems by explicitly considering water, ions, and lipids molecules. The intriguing perspective of simulating unbinding events, to retrieve mechanistic and energetic insight, is nevertheless limited because the majority of drug-like molecules remain bound to their biological target for a duration much longer than the MD capability (very small fragments may represent an exception⁸). Indeed, the RT of a molecule, can extend over several hours, while MD is usually limited to the micro - milliseconds timescale⁹. Computational chemists are developing MD protocols able to increase the sampling and therefore overcome this limitation. These algorithms can be classified as either enhanced or adaptive methods^{10,11}. The former are based on the simulated input of energy in order to facilitate the ligand transition from the energy minimum represented by the bound state to the unbound solvated configuration, and comprises metadynamics^{12,13} (in many different implementations¹⁴⁻¹⁶), steered MD¹⁷, accelerated MD^{18,19}, Gaussian-accelerated MD^{20,21}, random

accelerated MD²²⁻²⁴, smoothed potential MD²⁵, and replica exchange^{26,27}. One of the strengths of the enhanced sampling methods is the possibility to recover the energy surface of the dissociation by keeping track of the energy introduced. Weaknesses, on the other hand, can be the strong dependency on the user experience and the reliability of the mechanistic details retrieved, as some methods introduce atom positional restraints in order to restrain the secondary and ternary structures of the receptor²⁵. The adaptive sampling algorithms, instead, do not modify the Hamiltonian of the system but favor the sampling of less visited states by performing successive short simulations, according to the previous evolution of the system²⁸. The unbinding of the fragment benzamidine from the trypsin enzyme²⁹ represents a successful application of these approaches. More recent work on drug-like molecules employed the adaptive sampling method WExplore to simulate the dissociation and retrieve a quantitative kinetic description of the overall event³⁰⁻³².

In this work, we applied supervised MD (SuMD³³), an adaptive sampling method originally designed to speed up the simulation of binding events, to the unbinding of small molecules. SuMD was tested on seven different intermolecular complexes (Table 1 and Table S1) involving four G protein-coupled receptors (GPCRs), namely the orexin receptor 2 (OX₂R), the muscarinic 2 receptor (M₂R), the adenosine receptors A₁ (A₁R) and A_{2A} (A_{2A}R), and the cytosolic enzyme epoxide hydrolase (sEH). The GPCRs are a superfamily of membrane receptors³⁴ and represent the most clinically relevant target of commercialized drugs³⁵. To the best of our knowledge, this is the first reported unbiased MD method successfully applied to the unbinding of drug-like molecules from these fundamental pharmacological targets^{36,37}. SuMD outcomes were critically compared to the biased metadynamics method, highlighting the usefulness of the approach for the

mechanistic description of unbinding events, rather than for quantitative estimations of kinetics parameters.

METHODS

The supervised MD (SuMD) protocol for the unbinding

The supervised MD (SuMD) approach is an adaptive sampling method¹¹ so far employed for simulating the formation of intermolecular complexes in timescales that are one or two orders of magnitudes faster than the corresponding classic (unsupervised) simulations³³. Sampling is gained without the introduction of any energetic bias, by applying a tabu-like algorithm to monitor the distance between the centers of mass (or the geometrical centers) of the ligand and the predicted binding site. A series of short unbiased MD simulations are performed, and after each simulation the distances (collected at regular time intervals) are fitted to a linear function. If the resulting slope is negative (showing progress towards the target) the next simulation step starts from the last set of coordinates and velocities produced, otherwise the simulation is restarted by randomly assigning the atomic velocities. The SuMD has been successfully applied to study the binding mechanism of both small molecules and peptides^{33,38-44}.

Here we present a slightly modified version of the SuMD protocol that aims to simulate the unbinding of small molecules. As for the original binding version of the protocol, this is realized by supervising the inter-centroid distance and considering a short MD simulation as productive if at least one of the following criteria is realized:

- The slope of the fitted linear function has value ≥ 0

- The centroids distance at the end of the MD run has increased compared to the last productive short MD simulation

Differently from the original SuMD algorithm, the length (Δt) of the short simulations performed increases along the unbinding pathway, according to the formula:

$$\Delta t = \Delta t_0 N t_i \quad (2)$$

Δt_0 is the duration of the very first MD time window and $N t_i$ represents a factor that is picked from three user-defined values ($N t_1$, $N t_2$, and $N t_3$), according to the last ligand-protein distance detected. Three distance threshold values (D_1 , D_2 and D_3 - Table S2) are set and the ligand-protein distance (r_L) at the end of each MD run is compared to these threshold values, allowing a decision on the value of $N t_i$ factor according to the following conditions:

$$r_L \leq D_1 \rightarrow N t_i = 1 \quad (3)$$

$$D_1 < r_L \leq D_2 \rightarrow N t_i = N t_1 \quad (4)$$

$$D_2 < r_L \leq D_3 \rightarrow N t_i = N t_2 \quad (5)$$

$$D_3 < r_L \rightarrow N t_i = N t_3 \quad (6)$$

The goal of increasing the simulation time window (Δt in Equation 2) along the unbinding pathway is to facilitate the sampling of metastable states, which can otherwise be poorly visited as very short SuMD simulation time windows favor the escape from energy minima (the global minima is represented by the orthosteric ligand-protein complex). As reported in Table S2, different user-defined values have been tested and normally values of 3 Å, 5 Å and 8 Å are

appropriate for D₁, D₂ and D₃ respectively. Longer values are used for the orexin 2 and muscarinic 2 receptors because the ligands sit further from the receptor surface.

The SuMD unbinding is iterated until no ligand-protein van der Waals contact is detected by means of the GetContacts scripts tools (<https://getcontacts.github.io>). The distance between the ligand and the protein centers of masses (Table S3) was computed using PLUMED 2⁴⁵.

The supervised MD (SuMD) protocol for the adenosine binding to the A₁R.

To simulate the adenosine binding to the A₁R (Table S4) the distance between the centroid of the agonist and the centroid of the orthosteric residues N254^{6,55}, F171^{ECL2}, T277^{7,42}, and H278^{7,43} was supervised during 500 ns long time windows until it reached a value less than 3 Å.

Biological targets and ligand force field parameters

Four G protein-coupled receptors (GPCR) and one cytosolic protein were considered (a total of seven complexes - Table 1 and Table S1). The CHARMM36^{46,47}/CGenFF 3.0.1⁴⁸⁻⁵⁰ force field combination was employed in the molecular dynamics (MD) simulations performed in this work.

Initial ligand force field, topology and parameter files were obtained from the ParamChem webserver⁴⁸. Adenosine and NECA are already well-parameterized in the CGenFF force field. ZMA parameters were the same as our previous work⁵¹. The dihedral terms of TPPU and QNB were visually inspected during short MD simulations in water and no further optimization was performed. EMPA rotatable bonds associated with a higher ParamChem penalty were optimized at the HF/6-31G* level of theory using the Parameterize utility, which is part of the HTMD⁵² environment, after fragmentation of the molecule.

Table 1. The seven intermolecular complexes considered. The GPCRs are identified by the PDB codes 2YDO⁵³ (A_{2A} R in complex with adenosine), 6D9H⁵⁴ (A₁ R in complex with adenosine), 2YDV⁵³ (A_{2A} R in complex with the agonist NECA), 4EIY⁵⁵ (A_{2A} R bound to the inverse agonist ZMA), 5WQC⁵⁶ (OX₂ R in complex with the antagonist EMPA), and 3UON⁵⁷ (M₂ R in complex with QNB). The cytosolic system has PDB code 4OD0⁷ (sEH complexed with the inhibitor TPPU).

Protein	PDB code	Ligand	Ref
A2A receptor (A _{2A} R)	2YDO	adenosine	53
A1 receptor (A ₁ R)	6D9H	adenosine	54
A2A receptor (A _{2A} R)	2YDV	NECA	53
A2A receptor (A _{2A} R)	4EIY	ZMA	55
Orexin 2 receptor (OX ₂ R)	5WQC	EMPA	56
Muscarinic 2 receptor (M ₂ R)	3UON	QNB	57
Soluble epoxide hydrolase (sEH)	4OD0	TPPU	7

Protein preparation

The complete A_{2A}R structures (Table 1 and Table S1) were retrieved from the Adenosiland database⁵⁸. The intracellular loop 3 (ICL3) of the A₁ R and OX₂R was modelled using Modeller 9.19⁵⁹, while no attempt was made to rebuild the M₂R ICL3. Hydrogen atoms were added by means of the pdb2pqr⁶⁰ and propka⁶¹ software (considering a simulated pH of 7.0); the protonation of titratable side chains was checked by visual inspection. The resulting five receptors were separately inserted in a square 90 Å x 90 Å 1-palmitoyl-2-oleyl-sn-glycerol-3-phosphocholine (POPC) bilayer (previously built by using the VMD Membrane Builder plugin 1.1, Membrane Plugin, Version 1.1. at: <http://www.ks.uiuc.edu/Research/vmd/plugins/membrane/>), through an insertion method⁶², along with their co-crystallized ligand (and the water molecules within 5 Å of the ligand). The receptor orientation was obtained by superposing the coordinates on the

corresponding structure retrieved from the OPM database⁶³. Lipids overlapping the receptor transmembrane helical bundle were removed and TIP3P water molecules⁶⁴ were added to the simulation box by means of the VMD Solvate plugin 1.5 (Solvate Plugin, Version 1.5. at <<http://www.ks.uiuc.edu/Research/vmd/plugins/solvate/>). Finally, overall charge neutrality was reached by adding Na⁺/Cl⁻ counter ions up to the final concentration of 0.150 M), using the VMD Autoionize plugin 1.3 (Autoionize Plugin, Version 1.3. at <<http://www.ks.uiuc.edu/Research/vmd/plugins/autoionize/>).

The sodium ion was retained in the allosteric binding site^{55,65} of the A_{2A}R-ZMA complex⁶⁶ and the G_i protein α subunit helix H5 (residues 329 to 355) was kept in the intracellular side of the A₁R, in order to maintain the full-active conformation of the receptor.

The simulation box for the sEH-TPPU complex was prepared by titrating the protein and solvating the system as described above. One of the two domains of sEH was deleted and the remaining one renumbered consistently with ref.³².

Systems equilibration and general MD settings

The MD engine ACEMD⁶⁷ was employed for both the equilibration and productive simulations. The equilibration of the membrane systems was achieved in isothermal-isobaric conditions (NPT) using the Berendsen barostat⁶⁸ (target pressure 1 atm) and the Langevin thermostat⁶⁹ (target temperature 300 K) with low damping of 1 ps⁻¹. A four-stage procedure was performed (integration time step of 2 fs): first, clashes between protein and lipid atoms were reduced through 2000 conjugate-gradient minimization steps, then a 2 ns long MD simulation was run with a positional constraint of 1 kcal mol⁻¹ Å⁻² on protein and lipid phosphorus atoms. During the second stage, 20 ns of MD simulation were performed constraining only the protein atoms, while in the last

equilibration stage, positional constraints were applied only to the protein backbone alpha carbons, for a further 20 ns. Globular protein equilibration was achieved in two steps: after 500 cycles of conjugate-gradient minimization, the system was simulated for 5 ns, employing an integration time step of 2 fs, in the isothermal-isobaric conditions (NPT).

Productive trajectories (Table S4) were computed with an integration time step of 4 fs in the canonical ensemble (NVT). The target temperature was set at 300 K, using a thermostat damping of 0.1 ps^{-1} ; the M-SHAKE algorithm^{70,71} was employed to constrain the bond lengths involving hydrogen atoms. The cut-off distance for electrostatic interactions was set at 9 \AA , with a switching function applied beyond 7.5 \AA . Long range Coulomb interactions were handled using the particle mesh Ewald summation method (PME)⁷² by setting the mesh spacing to 1.0 \AA .

Metadynamics simulations

Metadynamics was performed on five out of seven complexes (Table S4). During metadynamics simulations a history-dependent energetic is virtually deposited along a predefined set of collective variables (CVs) that are able to describe the evolution of the system away from an energetic minimum. When this energetic biasing term is added, the probability that the system will revisit that specific configuration is decreased according to the shape of the supplied energetic Gaussian function. In this way it is possible to computationally fill energy minimum on the energy surface that is defined by the CVs, increasing the transition probability between different energy minima^{12,13}. Before performing a metadynamics simulation it is necessary to define one or more CVs able to describe the system transition of interest. Here, the Gaussian deposition was performed along the distances between the geometrical centers of the ligand and the protein (or a part of it - Table S3). The use of a similar ligand-receptor distance as CV during unbinding simulations has

been successfully applied⁷³ to class A GPCRs. We employed the well-tempered¹⁴ version of metadynamics: the starting height of the Gaussian energy terms was set at 0.01 kcal mol⁻¹, while the width was 0.1 Å, with depositions done every 2 ps using Plumed 2⁴⁵ as an ACEMD⁶⁷ plugin. The bias factor was set to 15 and the temperature to 300 K. The energy surfaces obtained by integrating the Gaussians deposited are reported in Figure S1.

Notably, the metadynamics simulations were not designed to fully reconstruct the unbinding energy surfaces (no convergence was reached during the three replicas performed - Figure S1), but to supply mechanistic insight for a direct comparison with SuMD.

Analysis of the MD trajectories

Interatomic contacts and root mean square deviations (RMSD) were computed using VMD⁷⁴. A contact was considered productive if the distance between two atoms was less than 3.5 Å. Ligand-protein hydrogen bonds were detected using the GetContacts scripts tool (<https://getcontacts.github.io>), setting a hydrogen bond donor-acceptor distance of 3.3 Å and an angle value of 150° as geometrical cut-offs. Contacts and hydrogen bond persistency are quantified as the percentage of frames (over all the frames obtained by merging the different replicas) in which protein residues formed contacts or hydrogen bonds with the ligand. The computation takes into account direct and water mediated interactions.

Distances between atoms were computed using PLUMED 2⁴⁵. Both the molecular mechanics Poisson-Boltzmann surface area (MM/PBSA) energy of the GPCR complexes (implicitly modelling the membrane using an heterogeneous dielectric constant) and the molecular mechanics energies combined with the generalized Born and surface area continuum solvation (MM/GBSA - for the sEH:TPPU complex) method were computed with the MMPBSA.py⁷⁵ script

(AmberTools17 suite at <http://ambermd.org/>), using the default settings, after transforming the CHARMM psf topology files to an Amber prmtop format using ParmEd (documentation. at <http://parmed.github.io/ParmEd/html/index.html>). We chose to compute the MM/PBSA and MM/GBSA energy also on the metadynamics trajectories to allow a direct comparison with the unbiased SuMD simulations. Detection of hydrated spots within the binding sites was performed on a 100 ns long classic MD simulations by means of AquaMMapS⁵¹.

Numbering system

Throughout the manuscript, the Ballesteros-Weinstein residues numbering system for the GPCRs⁷⁶ is adopted.

RESULTS

The A_{2A}R – adenosine complex

The A_{2A}R is a potential pharmaceutical target for the Parkinson's disease⁷⁷⁻⁷⁹ and numerous cancers⁸⁰. It is also one of the most characterized GPCRs as, to date, more than 40 X-ray and cryo-EM structures have been published⁸¹. In the bound state^{53,82} (Figure 1a) the adenosine forms key hydrogen bonds with A_{2A}R residues N253^{6,55}, S277^{7,42}, H278^{7,43}, a water mediated interactions with H250^{6,52}, and a π - π interaction that involves F168^{ECL2}. Moreover, in our simulations it forms a water-mediated interaction between the ribose ring and N181^{5,42}, but a direct hydrogen bond can occur.

Besides the orthosteric residues (Table S5, Table S6), during SuMD unbinding simulations (Video S1, Figure 1b) the A_{2A}R side chains I66^{2.64}, S67^{2.65}, I66^{2.64}, Y9^{1.35}, Y271^{7.36}, L267^{7.32}, V172^{ECL2}, L167^{ECL2}, S6^{1.32}, A81^{3.29}, T256^{6.58}, H264^{ECL3} and E13^{1.39} engaged in direct interactions with adenosine (Table S5, Table S6). E169^{ECL2} stabilized the ligand with hydrogen bonds and water-mediated interactions both in the bound state and throughout the dissociation. Interestingly, several SuMD replicas required the E169^{ECL2} - H264^{ECL3} salt bridge opening (Video S1 - in line with previously reported adenosine binding simulations³⁹) but this does not appear to be a fundamental step of the dissociation event. While the key hydrogen bond between adenosine and N253^{6.55} tended to form and break several times before the dissociations started, the almost simultaneous rupture of the buried hydrogen bonds formed with S277^{7.42}, H278^{7.43}, and N181^{5.42} appears to be the bottleneck of the unbinding (Video S1). In order to break these interactions, water molecules coming from the extracellular environment had first to hydrate either the solvent-exposed hydrogen bond with N253^{6.55} or the adenine scaffold (Figure S2). Water molecules involved came also from a hydrated region located in proximity to the ribose moiety and the N181^{5.42}, and H250^{6.52} side chains (Figure S2), or from within the transmembrane (TM) domain, in line with the water flux highlighted in the work from Lee *et al.*⁸³.

The above interaction pattern generally matches with the metadynamics results (Table S5, Table S6), but a direct comparison between the two methods shows that under the parameters used for these simulations, SuMD sampled more contacts at the extracellular vestibule of A_{2A}R (Y271^{7.36}, Y9^{1.35}, E13^{1.39}, E169^{ECL2}) than the metadynamics, which instead extensively explored interactions in the orthosteric site (Figure S3a,b). This is consistent with the points' distribution in the energy landscapes, as the metadynamics sampled more adenosine bound states (spread points at minima B Figure S3c) than SuMD did (narrow distribution of point at minima B Figure 1c).

Interestingly, while both methods simulated a common unbinding path (Figure 1d, Figure S3d) close to the extracellular loop 3 (ECL3), only SuMD explored an alternative route between the extracellular loop 2 (ECL2) and the top of transmembrane helix 1 (TM1) (Figure 1d).

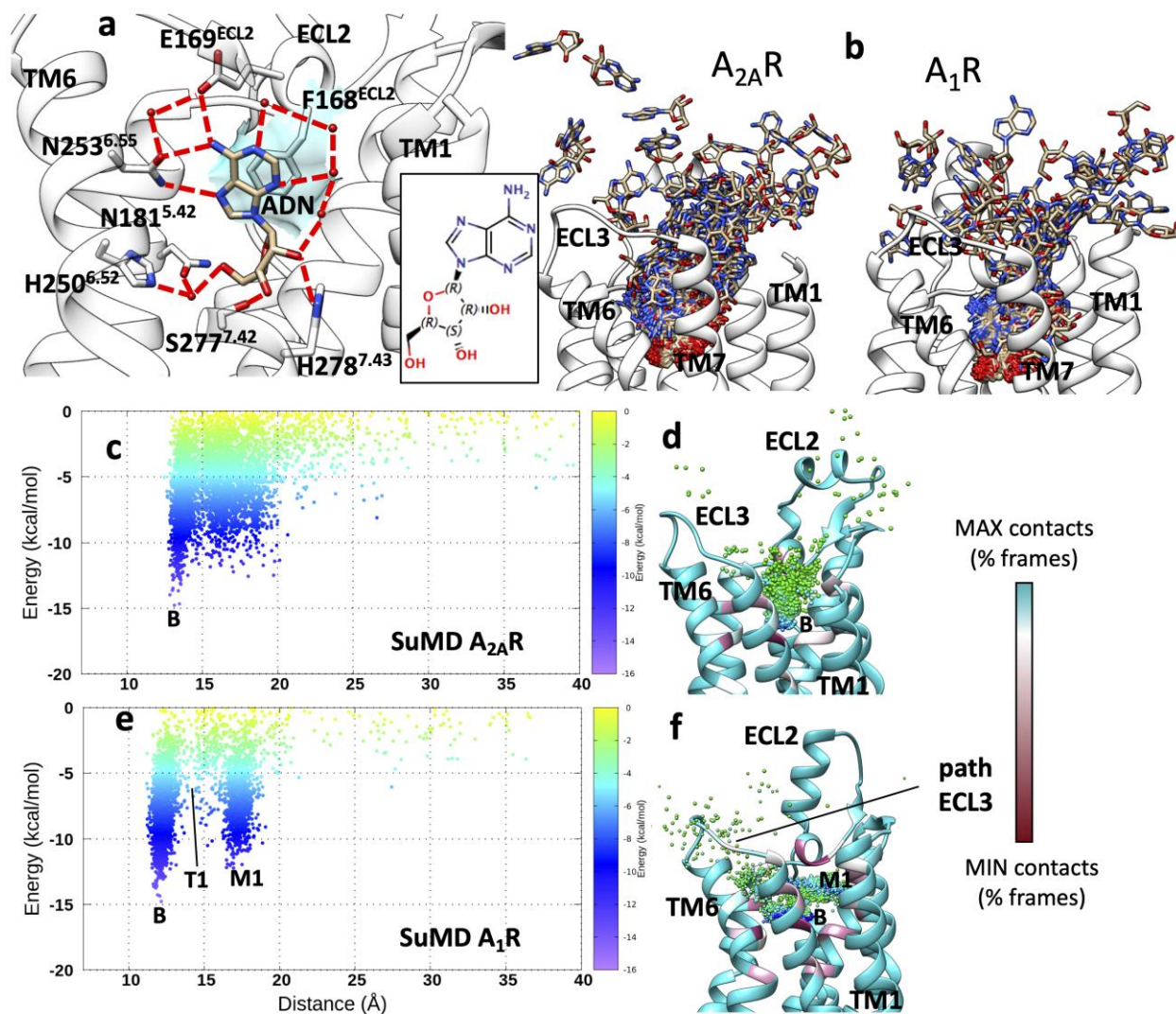


Figure 1. The adenosine unbinding from the A_{2A} and A_1 receptors. a) The $A_{2A}R$ - adenosine X-ray intermolecular complex⁵³. Water oxygen atoms within 3 Å from the ligand are shown in red. Hydrogen bonds are highlighted as dashed lines and hydrophobic interactions as a cyan transparent surface. The upper portion of TM7 has been removed for clarity. The 2D structure of

adenosine is reported in the box. **b)** A_{2A}R - adenosine (left panel) and A₁R - adenosine (right panel) unbinding configurations according to SuMD (the adenosine is shown every 1 ns of simulation as stick representation). **c)** A_{2A}R - adenosine unbinding energy landscape from SuMD simulations. **d)** adenosine centroids positions during SuMD, colored according to the energy interaction (MMPBSA energy < 0); the A_{2A}R is shown as ribbon and colored according to the overall contacts computed during SuMD simulations. **e)** A₁R - adenosine unbinding energy landscape from SuMD simulations. **f)** adenosine centroids positions during SuMD colored according to the energy interaction (MMPBSA energy < 0); the A₁R is shown as ribbon and colored according to the overall contacts computed during metadynamics simulations.

The A₁R – adenosine complex and the comparison with the SuMD binding simulations

The adenosine A₁ receptor (A₁R) is involved in ischemic disorders⁷⁹ and in the nociceptive transmission⁸⁴. The main orthosteric point mutations between A_{2A}R and A₁R are S67(A_{2A})^{2,65}N70(A₁), S277(A_{2A})^{7,42}T277(A₁), and M270(A_{2A})^{7,35}T270(A₁)⁸⁵, the latter contributing strongly to the A₁/A_{2A} ligand selectivity^{54,86}.

According to SuMD (Figure 1e, f, Video S2, Table S7 and Table S8), the S67(A_{2A})^{2,65}N70(A₁) mutation putatively modifies the energy landscape of the adenosine unbinding (Figure 1c, e) generating a further energy minimum (M1 in Figure 1e) a few Angstroms from the bound state (B in Figure 1c, e). Indeed, in contrast to the A_{2A}R, the ligand was forced to overcome transition configurations (T1 in Figure 1e) located between the bound state and the metastable state M1, where the adenosine hydrogen bonded with N70^{2,64} and N254^{6,55} side chains and formed hydrophobic contacts with F171^{ECL2} (Figure S4). At ECL3, the H264(A_{2A})^{ECL3}K265(A₁) mutation

potentially modifies the strength of the ionic interaction with E172^{ECL2} (E169^{ECL2} in A_{2A}), and possibly favored the adenosine unbinding towards the ECL3 path in A1R (Figure 1f) as a consequence of the narrower extracellular vestibule conformation.

We performed SuMD binding simulations (Video S3) to deliver insight from the possible differences between the adenosine – A₁R association and dissociation pathways (Figure S5). The binding routes sampled converged to a metastable site located at the top of TM5, TM5, the distal part of ECL2 and the proximal segment of ECL3. After stopping at this intermediate position, adenosine formed the orthosteric complex either passing between the E172^{ECL2} – K265^{ECL3} salt bridge during three replicas out of nine. This produced an energy landscape of the event characterized with two intermediate stable states (M_A and M_B in Figure S5a, b) characterized by stability comparable to the final one (state B in Figure S5a, b). Of note, the SuMD binding simulations were not combined with classic unsupervised MD to favor the sampling of the experimental binding pose³³ as we were interested in the non-equilibrium transition from the bulk solvent to the final binding site rather than reproducing the well-known final bound state. It is highly probable that the cryo-EM adenosine conformation would have produced a deeper energy minimum than state B did, justifying the spontaneous orthosteric binding of the ligand.

Interestingly, the adenosine binding and unbinding routes did not overlap (Figure S5c). This indicates a scenario that is not compliant with the principle of microscopic reversibility of binding. Such non-compliance has been proposed for processes in physiological non-equilibrium conditions like binding and protein folding^{87,88}.

The A_{2A}R – NECA complex

NECA is an adenosine synthetic analogue that bears an ethylcarboxamido moiety on the ribose 5'-oxydril group (Figure 2). This chemical modification brings the affinity for the A_{2A}R from the high to the low-nanomolar range, due to the introduction of two further hydrogen bonds (with T88^{3.36} and H250^{6.52} - Figure 2a, Table S9, Table S10) and the displacement of the water molecule that in the adenosine X-ray complex is placed in the proximity of N181^{5.42} and H250^{6.52} ⁸⁹. All the other orthosteric interactions characterizing the endogenous agonist are retained (Figure 2a, Table S9, Table S10).

In contrast to the adenosine simulations, NECA SuMD (Video S4, Figure 2) was more prone to sample interactions in the orthosteric site than the metadynamics, with the latter more able to explore contacts, hydrogen bonds and water-mediated interactions at the extracellular vestibule of the receptor (Figure S6a, b). The NECA propensity to remain in the binding site was driven by the direct hydrogen bond between the ligand ethylcarboxamido group and T88^{3.36} (Table S9, Table S10, and Figure S7). The rupture of this key interaction represented the bottleneck during the dissociation, as it occurred after the break of all the other hydrogen bonds (Figure S7) involving the ligand (e.g. the interactions with N253^{6.55}, E169^{ECL2}, S277^{7.42}, H250^{6.52} and H278^{7.43}) in all the SuMD replicas performed (Video S4). The effect of the NECA - T88^{3.36} hydrogen bond is evident also on the energy landscape of the unbinding (Figure 2c). The highly populated bound states (B in Figure 2c) are indeed markedly separated from the other states along the unbinding path by the poorly sampled state T1 (Figure 2c). Notably, there is no evident indication of this T88^{3.36}-related mechanistic step during metadynamics simulations (Figure S6c, Figure S7). The dynamics of the water molecules in the binding site suggests a shielding effect of the T88^{3.36} methyl, which protects the T88 hydrogen bond from hydration and therefore increases its persistency (Figure S8). This

scenario is in line with the proposed effect that buried hydrogen bonds may have on the overall kinetics of unbinding⁹⁰. Interestingly, the T88^{3.36}S mutation dramatically decreases NECA affinity for the A_{2A}R⁹¹, suggesting a marked increase in the kinetic of dissociation⁹⁰ (assuming the association rate k_{on} not affected).

Focusing on the rest of the unbinding paths, both during SuMD and metadynamics simulations NECA was able to reach the fully solvated state by transiently interacting with ECL3 (Figure 2d and Figure S6d). Subtle differences between the two methods are apparent at ECL2, where NECA made more metastable contacts with residues located at the helix portion of the loop according to the metadynamics (Figure S6d).

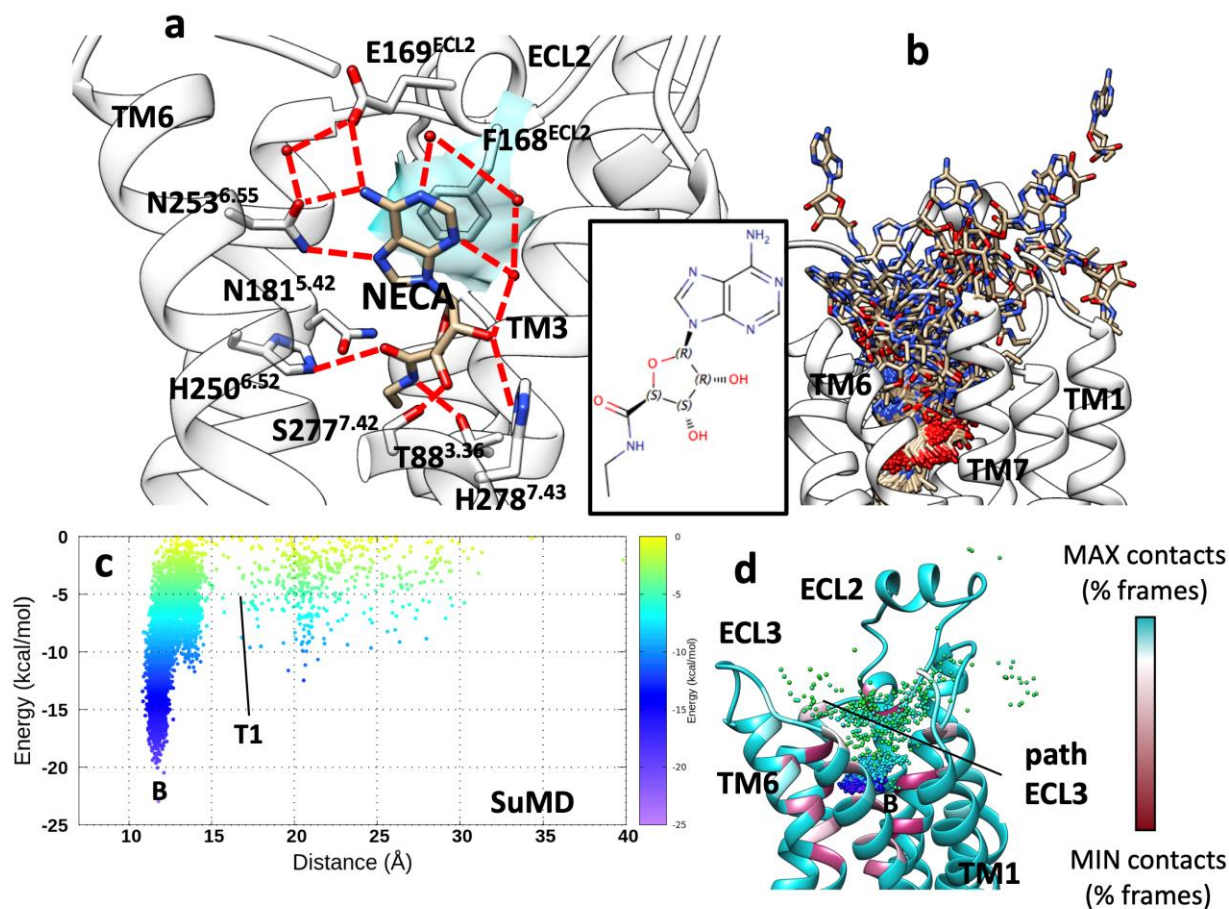


Figure 2. NECA unbinding from the A_{2A} receptor. **a)** The A_{2A}R - NECA X-ray intermolecular complex⁵³. Water oxygen atoms within 3 Å from the ligand are shown in red. Hydrogen bonds are highlighted as dashed lines and hydrophobic interactions as a cyan transparent surface. The upper portion of TM7 has been removed for clarity. The 2D structure of adenosine is reported in the box. **b)** A_{2A}R - NECA unbinding configurations according to SuMD (NECA is shown every 1 ns of simulation as stick representation). **c)** A_{2A}R - NECA unbinding energy landscape from SuMD simulations. **d)** NECA centroids positions during SuMD, colored according to the energy interaction reported in panel 2c (MMPBSA energy < 0); the A_{2A}R is shown as ribbon and colored according to the overall contacts computed during SuMD simulations.

The A_{2A}R – ZMA complex

ZMA is considered a prototypical A_{2A}R inverse agonist⁹². In the bound state (Figure 3a) the triazole-triazine bicyclic scaffold engages N253^{6.55} and E169^{ECL2} side chains via hydrogen bonds and makes hydrophobic contact with F168^{ECL2}, L249^{6.51}, H250^{6.52}, M270^{7.35} and I274^{7.39} (Figure 3a, Table S11, Table S12). The phenolic group, instead, orients towards the extracellular environment (but an alternative conformation interacting with the Y271^{7.36} side chain has been reported⁹³). The structural feature responsible of ZMA antagonistic activity is the absence of the ribose ring (characterizing the AR full agonists), as no interaction with the receptor key residues S277^{2.47} and H278^{2.48} is possible in the complex.

During SuMD unbinding simulations (Figure 3, Video S5), the antagonist made more interactions with the extracellular vestibule of the A_{2A} R than the adenosine and NECA (Figure S9a, b). More precisely, the phenolic ring engaged residues located at the top of TM2 (S67^{2.65}),

TM7 (L267^{7.32}), and L167^{ECL2} (Figure 3e), while the triazole-triazine scaffold was mainly responsible for interactions with ECL2 (E169^{ECL2}, S156^{ECL2}, Q157^{ECL2}, and K153^{ECL2}). In analogy with the work of Guo et al.²³, ZMA engaged the S156^{ECL2} and Q157^{ECL2} side chains (Table S11, Table S12, Figure S11a,b) with intermediate hydrogen bonds. Interestingly, the S156A^{ECL2} and Q157A^{ECL2} mutations do not affect the unbinding kinetics²³, indicating that the transition state of the event may occur earlier. The T256A^{6.58} and L267A^{7.32} mutations, on the other hand, strongly influence the unbinding kinetics of this ligand²³. Regarding the L267A^{7.32} mutant, a conformation of the ethylphenol group alternative to the one observed with L267^{7.32} has been proposed as a determinant for the residence time (RT) increase. The T256^{6.58}, H264^{ECL3} and E169^{ECL2} side chains are at the edge of a volume occupied by water molecules with low dynamicity, according to the AquaMMapS analysis⁵¹ (Figure S10). In this scenario, the T256A mutation may destabilize the H264^{ECL3} - E169^{ECL2} salt bridge, important for the unbinding kinetics of A_{2A}R antagonists⁹⁴, thereby triggering a decrease of RT (during SuMD simulations, ZMA dissociations occurred when the salt bridge was open). The opening of the salt bridge could also influence the key hydrogen bonds between N253^{6.55} and the antagonists (Figure S10), as the water molecule influx from the extracellular environment may favor its rupture.

Comparing the dissociation mechanisms obtained from SuMD and metadynamics, relevant differences can be observed at the extracellular vestibule of the receptor (Figure S11a,b), where ZMA engaged residues located at the ECL2 helix (S156^{ECL2}, Q157^{ECL2}, and K153^{ECL2}) in metastable interactions (states M_{ECL2} in Figure 3c, d) according to SuMD. During metadynamics, on the other hand, ZMA was more prone to sample intermediate states in the orthosteric site (as indicated by the wide distribution of points in Figure S11c and usually left the binding site by ECL3, or through a narrow path in the proximity of the central segment of ECL2 (Figure S11d).

The SuMD energy landscape (Figure 3c) highlights a clear discontinuity (T1 in Figure 3c) between the orthosteric bound states (B in Figure 3c) and the successive metastable states (M_{ECL2} in Figure 3c), due to the almost simultaneous break of the polar interactions with $N253^{6.55}$ and $E169^{ECL2}$ side chains (Video S5).

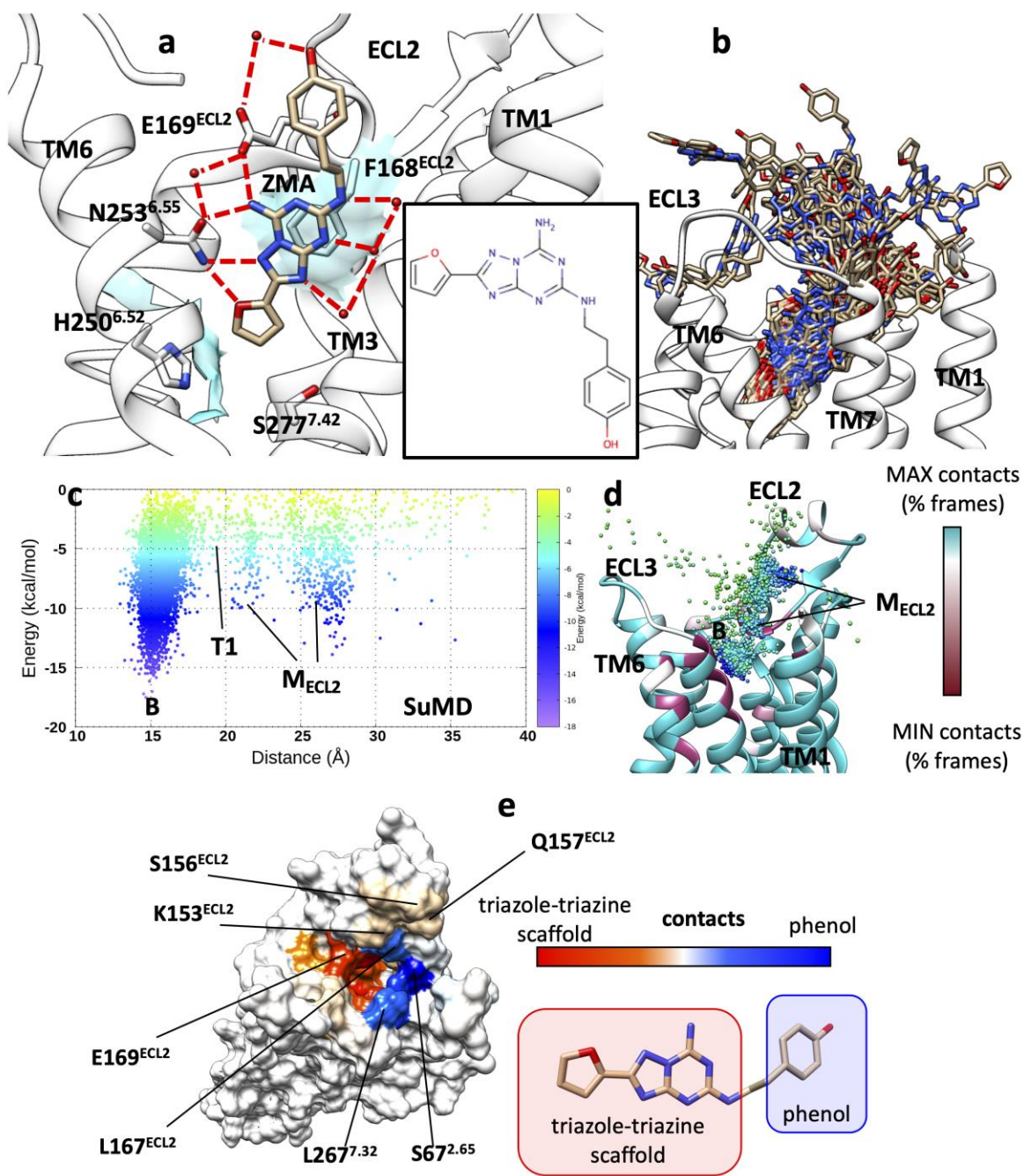


Figure 3. ZMA unbinding from the A_{2A} receptor. **a)** The A_{2A}R - ZMA X-ray intermolecular complex⁵⁵. Water oxygen atoms within 3 Å from the ligand are shown in red. Hydrogen bonds are highlighted as dashed lines and hydrophobic interactions as a cyan transparent surface. The upper portion of TM7 has been removed for clarity. The 2D structure of ZMA is reported in the box. **b)** A_{2A}R - ZMA unbinding configurations according to SuMD (ZMA is shown every 1 ns of simulation as stick representation). **c)** A_{2A}R - ZMA unbinding energy landscape from SuMD simulations. **d)** ZMA centroids positions during SuMD, colored according to the energy interaction reported in panel 3c (MMPBSA energy < 0); the A_{2A}R is shown as ribbon and colored according to the overall contacts computed during SuMD simulations **e)** A_{2A}R - ZMA SuMD contacts map colored according to the structural moiety of the ligand involved; in red and orange are shown the residues that mainly interacted with the triazole-triazine scaffold, while in blue are highlighted residues that mainly made contacts with the phenol group (white surface indicates either the same amount of contacts or no interactions at all).

The OX₂R – EMPA complex

Antagonizing the orexin-2 receptor (OX₂R) is considered a valuable therapeutic approach for the treatment of narcolepsy⁹⁵. The recent X-ray structure of the OX₂R in complex with the antagonist EMPA⁵⁶ has shed light on subtype selectivity and shown that in the bound state (Figure 4a) the ligand is not stabilized by direct hydrogen bonds. A water-mediated interaction is formed between Q134^{3,32} and the two nitrogen atoms of each pyridine ring of EMPA, and a further water-mediated hydrogen bond is formed between the carbonyl oxygen of the ligand and the H350^{7,39} side chain.

Moreover, EMPA forms numerous van der Waals contacts with T111^{2.61}, V138^{3.36}, F227^{5.42}, I320^{6.51}, S321^{6.52}, N324^{6.55}, H350^{7.39}, and Y354^{7.43}.

SuMD (Figure 4, Video S6) confirmed the low tendency of EMPA to form direct hydrogen bonds with the receptor along the unbinding path (except for Q187^{4.60}, which was engaged in intermediate states – Table S13, Table S14, Figure S12a, b). Interestingly, ECL2 and the N-terminal helix of the receptor chaperoned the ligand during the three replicas sampled (Figure 4b, Video S6), suggesting an important role in intermediate stabilization of the ligand. Ligand solvation has been suggested to contribute strongly to unbinding transition states⁹⁶ and, possibly, the OX₂R extracellular vestibule drives EMPA dissociation providing several hydrophobic contacts, and therefore gradual hydration before reaching the bulk. SuMD had the tendency to sample more metastable states located in proximity to the orthosteric site (Figure S12a, b), while during metadynamics simulations EMPA formed more contacts with the extracellular vestibule of the OX₂R (Figure S12a, b). Outcomes from SuMD (Video S6) indicated an overall EMPA unbinding mechanism (Figure S13) according to which the first step of the dissociation is the reorientation of the pyridine ring from the TM bundle core towards the top of TM7/ECL3 (step 1 in Figure S13a). This conformational change leads to transitory interactions with H350^{7.39} and residues located at the top of TM6 (K327^{6.58} in Figure S13a) and TM7 (F346^{7.35} in Figure S13a). The second step is proposed to be the EMPA transition to the extracellular vestibule of the receptor, where it forms several hydrophobic contacts with ECL2 and ECL3 (Figure S13b). During Step 3 the inhibitor interacts with the N terminal helix and the distal portion of ECL2 (Figure S13c) before completely unbinding. The energy surface from SuMD simulations shows a discontinuity (T₁ in Figure 4c) between the bound state (B in Figure 4c, d) and the metastable states at the ECL2 (M_{ECL2} in Figure 4c, d), which corresponds to step 2 of the simulated dissociation mechanism. This

transition putatively drives the overall kinetics of the event, as EMPA experienced a possibly energetic-unfavorable sudden solvation (Figure S14).

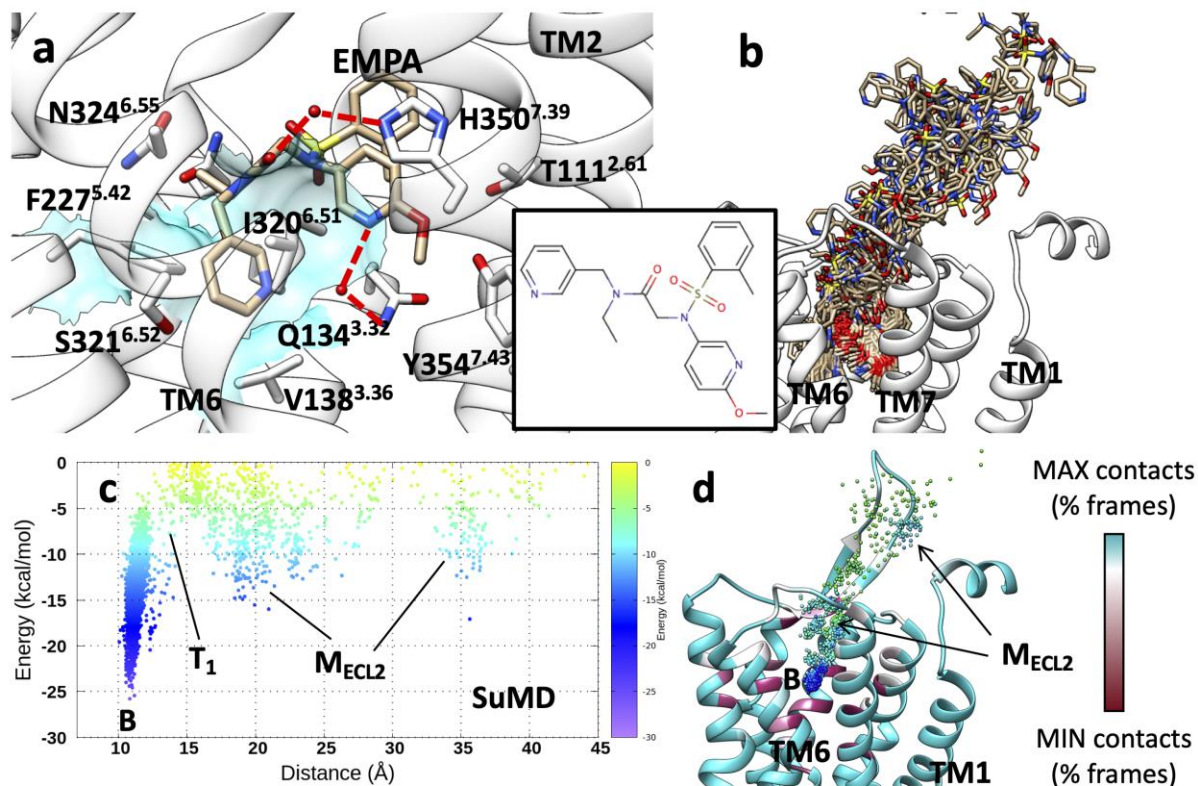


Figure 4. EMPA unbinding from the OX₂ receptor. **a)** The OX₂R- EMPA X-ray intermolecular complex⁵⁵. Water oxygen atoms within 3 Å from the ligand are shown in red. Hydrogen bonds are highlighted as dashed lines and hydrophobic interactions as a cyan transparent surface. The upper portion of TM7 has been removed for clarity. The 2D structure of EMPA is reported in the box. **b)** OX₂R – EMPA unbinding configurations according to SuMD (EMPA is shown every 1 ns of simulation as stick representation). **c)** OX₂R - EMPA unbinding energy landscape from SuMD simulations. **d)** EMPA centroids positions during SuMD, colored according to the energy interaction reported in panel 4c (MMPBSA energy < 0); the OX₂R is shown as ribbon and colored according to the overall contacts computed during SuMD simulations.

The M₂R – QNB complex

The five muscarinic receptors (M₁₋₅R) modulate the effects of the acetylcholine in both the central and parasympathetic nervous systems, with possible therapeutic repercussion on schizophrenia, Alzheimer's and Parkinson's diseases⁹⁷. However, the development of selective orthosteric drugs has been always complicated by the high degree of identity that characterizes the canonical binding site for these receptors. The inactive structure of the subtype M₂ was first solved through X-ray crystallography⁵⁷, delivering insights on the complex with the antagonists 3-quinuclidinyl benzilate (QNB). QNB binds in a buried pocket that is separated from the extracellular vestibule by the aromatic side chains of three tyrosine residues (Y104^{3,33}, Y403^{6,51}, and Y426^{7,39}). A charge-charge interaction with D103^{3,32} and a hydrogen bonds with N404^{6,52} orient the ligand in the binding site (Figure 5a), where a set of further hydrophobic contacts with F181^{ECL2}, T190^{5,42}, V111^{3,40}, and W400^{6,48} completes the interaction pattern. The deep position in the receptor TM core contributes to its strong binding (K_D in the picomolar range) and makes it a challenging test case for SuMD.

Five unbinding simulations were sampled. As a general view, QNB dissociated following a straight route between ECL2 and ECL3 (Figure 5b, Video S7, Table S15 and Table S16) but experiencing two major metastable states indicated with (M₁ and M₂ in Figure 5c and d, Figure S15 and Figure S16). In M₁ the antagonist slightly rotated, reorienting the two phenyl groups towards the extracellular vestibule (Figure S15a), and it tended to break the polar interactions with D103^{3,32} and N404^{6,52}. The T187^{5,39}A mutation has been reported as slightly decreasing QNB affinity for M₂R⁹⁸ and possibly indicates that the transition state along the unbinding occurs in the proximity of the orthosteric site. Metastable state M₂ (Figure S15b) was characterized by

electrostatic interaction with the T187^{5,39} side chain and several hydrophobic contacts with residues located at ECL2 and the top of TM6 and TM7.

Several analogies can be found with the previously reported biased unbinding simulations of tiotropium from the M₃R subtype⁹⁹. Kruse and collaborators indeed, proposed a linear unbinding path characterized by two metastable states above the orthosteric site.

Given the reduced length of the MR_s ECL2 and ECL3, which do not protrude towards the solvent bulk phase, it is not surprising that the allosteric sites reported so far^{100–102} are topologically situated over the canonical orthosteric one and are defined by several side chains from the loops as well as the top of all the TMD. Among these, W422^{7,35} has been suggested to populate two rotameric conformations, responsible for orienting the indole horizontally (parallel to the membrane surface) or vertically (normal to the membrane surface). Four SuMD replicas out of five suggest that the planar orientation would favor the unbinding, contributing to the stabilization of the outgoing ligand.

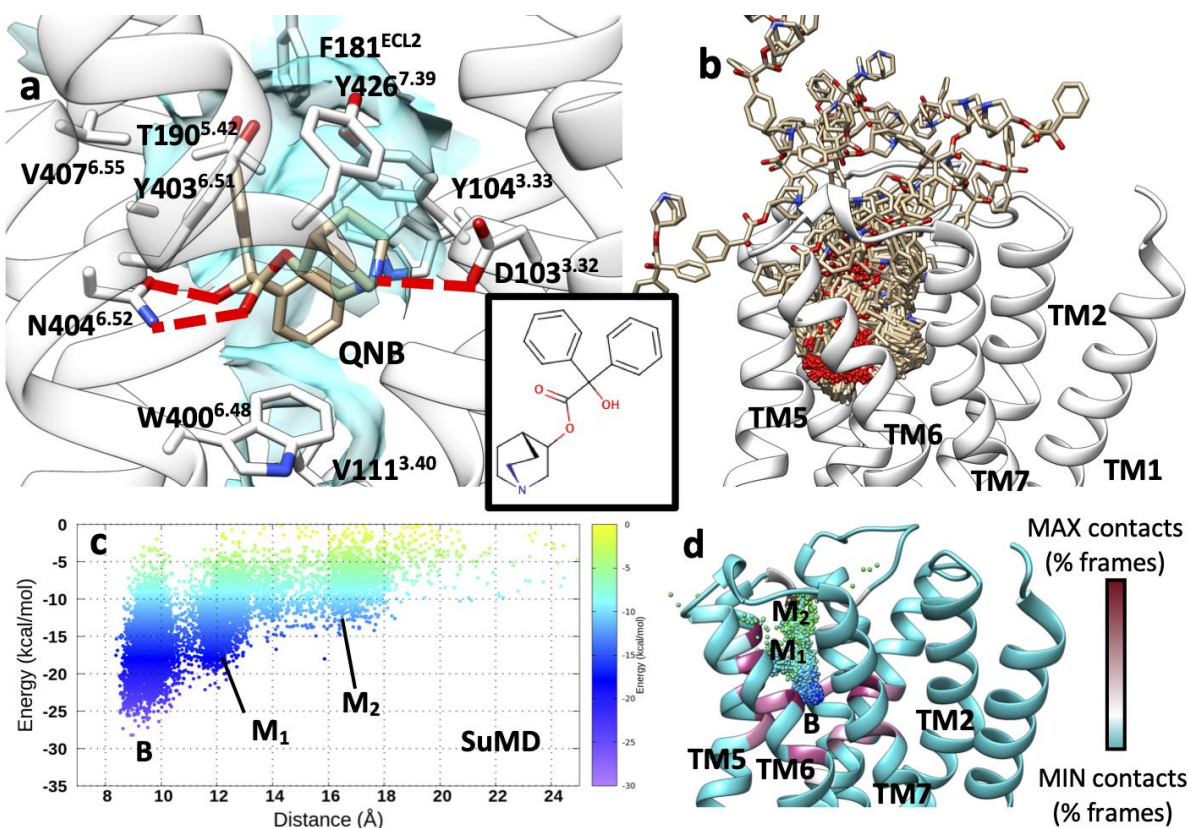


Figure 5. QNB unbinding from the M₂ R. **a)** The M₂R- QNB X-ray intermolecular complex⁵⁷. Hydrogen bonds are highlighted as dashed lines and hydrophobic interactions as a cyan transparent surface. The top of TM1 and TM2 have been removed for clarity. The 2D structure of QNB is reported in the box. **b)** M₂R –QNB unbinding configurations according to SuMD (QNB is shown every 1 ns of simulation as stick representation). **c)** M₂R – QNB unbinding energy landscape from SuMD simulations. **d)** QNB centroids positions during SuMD, colored according to the energy interaction reported in panel 5c (MMPBSA energy < 0); the M₂R is shown as ribbon and colored according to the overall contacts computed during SuMD simulations.

The sEH – TPPU complex

The soluble epoxide hydrolase (sEH) is a cytosolic enzyme responsible of the hydrolysis of epoxyeicosatrienoic acids (EETs) to the corresponding dihydroxyeicosatrienoic acids (DHETs)¹⁰³. Given the anti-inflammatory action of EETs¹⁰⁴, pharmaceutical strategies able to inhibit the sEH action should be beneficial in modulating acute inflammatory disorders¹⁰⁵. Among the various scaffolds designed, the 1,3-disubstituted urea has been so far characterized as the most potent in inhibiting sEH¹⁰⁶.

SuMD unbinding replicas (Figure 6, Video S8) were collected using the X-ray crystal structure of sEH in complex with the derivative 1-trifluoromethoxyphenyl-3-(1-propionylpiperidin-4-yl)-urea (TPPU)⁷. In the active site (Figure 6a), TPPU engages the key residues D105, Y236, and Y153 in hydrogen bonds, while hydrophobic contacts are formed with Y37, F157, L178, M189, L198 and the trifluoromethoxy group.

The dissociation of this complex was recently investigated³² by means of the WExplore algorithm³¹, allowing a direct comparison with our proposed method. Both the SuMD (Table S17, TableS18, Figure S17a, b, and Video S8) and the metadynamics (Figure S17a, b) highlighted the rupture of the hydrogen bond with D105 as the first step of the unbinding (Figure 6b). During this preliminary event, the urea carbonyl oxygen of TPPU was involved in a stabilizing hydrogen bond network with Y236, Y153 and N154 (M_1 in Figure 6d, e, and Video S8). Successively, in analogy to the results from Dickson *et al*³², the inhibitor experienced two possible dissociation paths (Figure 6c, Video S8). Along Path A (Figure 6c, e) the inhibitor was chaperoned by a hydrogen bond with Y153 and experienced a rotation necessary to orient the structure towards the molecular gate where it sampled transitory metastable states (M_A in Figure 6d) interacting with M189, L187,

and L178 (Table S17, Table S18). Path B (Figure 6c, e), instead, was mainly characterized by intermediate interactions with S247 and M109 (metastable states M_B in Figure 6d, e) and did not require a major reorientation of the ligand, already appropriately oriented in the bound state.

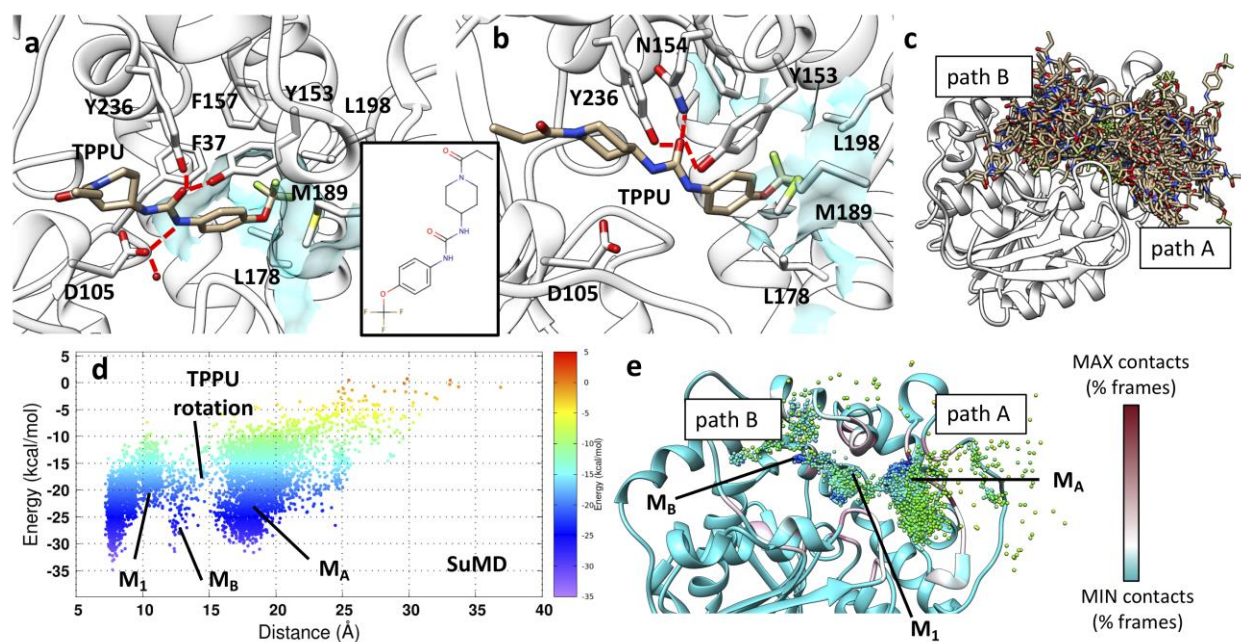


Figure 6. TPPU unbinding from the sEH enzyme. **a)** The sEH - TPPU X-ray intermolecular complex⁵³. Water oxygen atoms within 3 Å from the ligand are shown in red. Hydrogen bonds are highlighted as dashed lines and hydrophobic interactions as a cyan transparent surface. The 2D structure of TPPU is reported in the box. **b)** First step of unbinding, common to both path A and path B; **c)** TPPU unbinding configurations according to four SuMD replicas (the TPUU position is shown every 1 ns of simulation); the ligand dissociation takes place through two main paths: along path A the inhibitor is stabilized mainly through interactions with M189, while path B is less characterized by metastable states, and requires shorter simulations (Video S8). **d)** sEH - TPPU unbinding energy landscape from SuMD simulations. **e)** TPPU centroid positions during SuMD, colored according to the energy interaction reported in panel 6d (MMGBSA energy < 0); the sEH

is shown as ribbon and colored according to the overall contacts computed during SuMD simulations.

CONCLUSION

In the present work, the SuMD protocol was applied to simulate the unbiased dissociation of a set of small molecules from four GPCRs (the A₁R, A_{2A}R, the M₂R, and the OX₂R) and a globular protein (the enzyme sEH). The GPCRs covered all the three conformations so far experimentally reported: the inactive (the A_{2A}R – ZMA, the M₂R – QNB, and the OX₂R – EMPA complexes), the intermediate active (the A_{2A}R – adenosine complex), and the fully active one (the A₁R – adenosine complex). The ligands considered are characterized by a residence time (RT) of several minutes (more than one hour in the case of ZMA) and include QNB, which is one of the most strongly binding GPCR antagonists with a K_D in the picomolar range¹⁰⁷.

As a general view, SuMD and the metadynamics sampled similar unbinding pathways, with the ligand usually experiencing more than one possible exit pathway (except for QNB and EMPA, which dissociated respectively from the M₂R and the OX₂R through one main route). The mechanisms proposed by the two methods differ in magnitude of the intermolecular contacts, the hydrogen bonds and the water-mediated interactions. Further divergences can be spotted in the energy landscapes of the dissociation events: SuMD was overall able to better reconstruct the multistep nature of the ligand-receptor dissociations by sampling heterogeneous metastable states, allowing hypotheses regarding the possible kinetic bottlenecks on the unbinding pathway.

This was particularly evident in the case of the NECA, whose dissociation from the A_{2A}R was strongly driven by the hydrogen bond with T88^{3,36}. Notably, the metadynamics protocol here employed relied only on the ligand-receptor distance metric, to permit a direct comparison with SuMD. The introduction of a further biased collective variable during metadynamics (decided according to *a priori* knowledge of the biological target considered) could dramatically increase the level of details achievable.

A remarkable aspect of the EMPA-OX₂R complex is the absence of direct protein-ligand hydrogen bonds. We have reported a proposed unbinding mechanism for EMPA, according to which three main steps occur. Even if the ligand translocation from the orthosteric site to the extracellular vestibule has been pointed out as the possible bottleneck of the event, the initial reorientation of the pyridyl ring (step 1 in Figure 5) allows the water molecules to start solvating the complex. Therefore, chemical modification able to restrain the conformational space of this substituent may increase the RT on this biological target.

The TPPU-sEH complex represented an important benchmark for SuMD, as its unbiased dissociation was recently simulated by the WExplore algorithm³². Overall, SuMD sampled a dissociation mechanism that highly resembled the one obtained from WExplore, as two different main unbinding routes were proposed. Unlike WExplore, the SuMD approach in this current implementation does not allow for quantitative estimations of kinetics parameters. However, recent computational protocols suggest the possibility of rescaling the simulation time to kinetically rank similar compounds^{22,108}. A straightforward approach could rely on the evaluation of both the total and the productive SuMD simulation time needed for dissociating structurally related compounds. SuMD could be also combined with other adaptive sampling methods to obtain a thorough sampling of both binding and unbinding, allowing the construction of kinetic Markov

state models. Besides, SuMD output may represent suitable references for metadynamics simulations based on path collective variable^{109,110}, which are capable to reconstruct the energy surface of the transitions.

In the future, given the immense chemical space and all the ligand-receptor interaction patterns possible, the SuMD approach should be tested on an extended number of different systems, comprised those whose unbinding is kinetically driven by major conformational rearrangements of the protein. Moreover, to facilitate the use of the protocol, future efforts should be addressed to simplify the user-defined settings, implementing a linear scaling of the time windows duration along the dissociation path.

According to SuMD and as a general view, the main bottlenecks of the dissociation from the class A GPCRs considered here occurred during early stages of the unbinding. This corroborates the importance of the stability of the ground state, represented by the bound complex, in modulating the energy of the transition states along the pathway and, in turn, the overall kinetics and the RT. The two distinct unbinding routes of TPPU, on the other hand, shared a common first dissociation step but were then characterized by different putative bottlenecks. Reasonably, these two molecular mechanisms can contribute to the overall kinetics with different weights, as one could occur faster than the other (i.e. could be kinetically favored).

In conclusion, the SuMD approach is a useful unbiased tool for computationally describing both the binding and the unbinding mechanism of drug-like molecules from important biological targets, such as the GPCRs. In light of its simple algorithm, it can be further developed and easily incorporated in any computational drug design pipeline to rationalize existing data and to produce new working hypothesis on the whole (un)binding process.

ASSOCIATED CONTENT

Supporting Information.pdf: Videos S1-S8 captions; Supplementary Tables S1-S18;
Supplementary Figures S1-S17

Video S1.mp4

Video S2.mp4

Video S3.mp4

Video S4.mp4

Video S5.mp4

Video S6.mp4

Video S7.mp4

Video S8.mp4

AUTHOR INFORMATION

Corresponding Authors

gd17863@essex.ac.uk

Author Contributions

The manuscript was written through contributions of all authors. All authors have given approval to the final version of the manuscript.

Funding Sources

CAR and GD received funding from Leverhulme Trust Grant RPG-2017-255.

Notes

The authors declare no competing financial interest.

Bibliography

- (1) Schuetz, D. A.; de Witte, W. E. A.; Wong, Y. C.; Knasmueller, B.; Richter, L.; Kokh, D. B.; Sadiq, S. K.; Bosma, R.; Nederpelt, I.; Heitman, L. H.; Segala, E.; Amaral, M.; Guo, D.; Andres, D.; Georgi, V.; Stoddart, L. A.; Hill, S.; Cooke, R. M.; De Graaf, C.; Leurs, R.; Frech, M.; Wade, R. C.; de Lange, E. C. M.; IJzerman, A. P.; Müller-Fahrnow, A.; Ecker, G. F. Kinetics for Drug Discovery: An Industry-Driven Effort to Target Drug Residence Time. *Drug Discov. Today* **2017**, *22*, 896–911.
- (2) Klein Herenbrink, C.; Sykes, D. A.; Donthamsetti, P.; Canals, M.; Coudrat, T.; Shonberg, J.; Scammells, P. J.; Capuano, B.; Sexton, P. M.; Charlton, S. J.; Javitch, J. A.; Christopoulos, A.; Lane, J. R. The Role of Kinetic Context in Apparent Biased Agonism at GPCRs. *Nat. Commun.* **2016**, *7*, 10842.
- (3) Lane, J. R.; May, L. T.; Parton, R. G.; Sexton, P. M.; Christopoulos, A. A Kinetic View of GPCR Allosterity and Biased Agonism. *Nat. Chem. Biol.* **2017**, *13*, 929–937.
- (4) Soethoudt, M.; Hoorens, M. W. H.; Doelman, W.; Martella, A.; van der Stelt, M.; Heitman, L. H. Structure-Kinetic Relationship Studies of Cannabinoid CB2 Receptor Agonists Reveal Substituent-Specific Lipophilic Effects on Residence Time. *Biochem. Pharmacol.* **2018**, *152*, 129–142.
- (5) Copeland, R. A.; Pompliano, D. L.; Meek, T. D. Drug-Target Residence Time and Its Implications for Lead Optimization. *Nat. Rev. Drug Discov.* **2006**, *5*, 730–739.
- (6) Guo, D.; Mulder-Krieger, T.; IJzerman, A. P.; Heitman, L. H. Functional Efficacy of Adenosine A_{2A} Receptor Agonists Is Positively Correlated to Their Receptor Residence Time. *Br. J. Pharmacol.* **2012**, *166*, 1846–1859.
- (7) Lee, K. S. S.; Liu, J.-Y.; Wagner, K. M.; Pakhomova, S.; Dong, H.; Morisseau, C.; Fu, S. H.; Yang, J.; Wang, P.; Ulu, A.; Mate, C. A.; Nguyen, L. V.; Hwang, S. H.; Edin, M. L.; Mara, A. A.; Wulff, H.; Newcomer, M. E.; Zeldin, D. C.; Hammock, B. D. Optimized Inhibitors of Soluble Epoxide Hydrolase Improve in Vitro Target Residence Time and in Vivo Efficacy. *J. Med. Chem.* **2014**, *57*, 7016–7030.
- (8) Huang, D.; Caflisch, A. The Free Energy Landscape of Small Molecule Unbinding. *PLoS Comput. Biol.* **2011**, *7*, e1002002.
- (9) Kohlhoff, K. J.; Shukla, D.; Lawrenz, M.; Bowman, G. R.; Konerding, D. E.; Belov, D.; Altman, R. B.; Pande, V. S. Cloud-Based Simulations on Google Exacycle Reveal Ligand Modulation of GPCR Activation Pathways. *Nat. Chem.* **2014**, *6*, 15–21.
- (10) De Vivo, M.; Masetti, M.; Bottegoni, G.; Cavalli, A. Role of Molecular Dynamics and Related Methods in Drug Discovery. *J. Med. Chem.* **2016**, *59*, 4035–4061.
- (11) Deganutti, G.; Moro, S. Estimation of Kinetic and Thermodynamic Ligand-Binding Parameters Using Computational Strategies. *Future Med. Chem.* **2017**, *9*, 507–523.
- (12) Laio, A.; Parrinello, M. Escaping Free-Energy Minima. *Proc. Natl. Acad. Sci. USA* **2002**, *99*, 12562–12566.
- (13) Barducci, A.; Bonomi, M.; Parrinello, M. Metadynamics. *WIREs Comput Mol Sci* **2011**, *1*, 826–843.
- (14) Barducci, A.; Bussi, G.; Parrinello, M. Well-Tempered Metadynamics: A Smoothly Converging and Tunable Free-Energy Method. *Phys. Rev. Lett.* **2008**, *100*, 020603.
- (15) Pramanik, D.; Smith, Z.; Kells, A.; Tiwary, P. Can One Trust Kinetic and Thermodynamic Observables from Biased Metadynamics Simulations: Detailed

- Quantitative Benchmarks on Millimolar Drug Fragment Dissociation. *J. Phys. Chem. B* **2019**, *123*, 3672–3678.
- (16) Valsson, O.; Tiwary, P.; Parrinello, M. Enhancing Important Fluctuations: Rare Events and Metadynamics from a Conceptual Viewpoint. *Annu. Rev. Phys. Chem.* **2016**, *67*, 159–184.
- (17) Izrailev, S.; Stepaniants, S.; Israilewitz, B.; Kosztin, D.; Lu, H.; Molnar, F.; Wriggers, W.; Schulten, K. Steered Molecular Dynamics. In *Computational molecular dynamics: challenges, methods, ideas*; Deuffhard, P.; Hermans, J.; Leimkuhler, B.; Mark, A. E.; Reich, S.; Skeel, R. D., Eds.; Lecture notes in computational science and engineering; Springer Berlin Heidelberg: Berlin, Heidelberg, 1999; Vol. 4, pp. 39–65.
- (18) Hamelberg, D.; Mongan, J.; McCammon, J. A. Accelerated Molecular Dynamics: A Promising and Efficient Simulation Method for Biomolecules. *J. Chem. Phys.* **2004**, *120*, 11919–11929.
- (19) Perez, D.; Uberuaga, B. P.; Shim, Y.; Amar, J. G.; Voter, A. F. Chapter 4 Accelerated Molecular Dynamics Methods: Introduction and Recent Developments. In; Annual reports in computational chemistry; Elsevier, 2009; Vol. 5, pp. 79–98.
- (20) Miao, Y.; Bhattarai, A.; Nguyen, A. T. N.; Christopoulos, A.; May, L. T. Structural Basis for Binding of Allosteric Drug Leads in the Adenosine A1 Receptor. *Sci. Rep.* **2018**, *8*, 16836.
- (21) Miao, Y.; McCammon, J. A. Mechanism of the G-Protein Mimetic Nanobody Binding to a Muscarinic G-Protein-Coupled Receptor. *Proc. Natl. Acad. Sci. USA* **2018**, *115*, 3036–3041.
- (22) Kokh, D. B.; Amaral, M.; Bomke, J.; Grädler, U.; Musil, D.; Buchstaller, H.-P.; Dreyer, M. K.; Frech, M.; Lowinski, M.; Vallee, F.; Bianciotto, M.; Rak, A.; Wade, R. C. Estimation of Drug-Target Residence Times by τ -Random Acceleration Molecular Dynamics Simulations. *J. Chem. Theory Comput.* **2018**, *14*, 3859–3869.
- (23) Guo, D.; Pan, A. C.; Dror, R. O.; Mocking, T.; Liu, R.; Heitman, L. H.; Shaw, D. E.; IJzerman, A. P. Molecular Basis of Ligand Dissociation from the Adenosine A2A Receptor. *Mol. Pharmacol.* **2016**, *89*, 485–491.
- (24) Peräkylä, M. Ligand Unbinding Pathways from the Vitamin D Receptor Studied by Molecular Dynamics Simulations. *Eur Biophys J* **2009**, *38*, 185–198.
- (25) Mollica, L.; Decherchi, S.; Zia, S. R.; Gaspari, R.; Cavalli, A.; Rocchia, W. Kinetics of Protein-Ligand Unbinding via Smoothed Potential Molecular Dynamics Simulations. *Sci. Rep.* **2015**, *5*, 11539.
- (26) Sugita, Y.; Okamoto, Y. Replica-Exchange Molecular Dynamics Method for Protein Folding. *Chem. Phys. Lett.* **1999**, *314*, 141–151.
- (27) Fukunishi, H.; Watanabe, O.; Takada, S. On the Hamiltonian Replica Exchange Method for Efficient Sampling of Biomolecular Systems: Application to Protein Structure Prediction. *J. Chem. Phys.* **2002**, *116*, 9058.
- (28) Doerr, S.; De Fabritiis, G. On-the-Fly Learning and Sampling of Ligand Binding by High-Throughput Molecular Simulations. *J. Chem. Theory Comput.* **2014**, *10*, 2064–2069.
- (29) Plattner, N.; Noé, F. Protein Conformational Plasticity and Complex Ligand-Binding Kinetics Explored by Atomistic Simulations and Markov Models. *Nat. Commun.* **2015**, *6*, 7653.
- (30) Dickson, A. Mapping the Ligand Binding Landscape. *BioRxiv* **2018**.

- (31) Dickson, A.; Lotz, S. D. Multiple Ligand Unbinding Pathways and Ligand-Induced Destabilization Revealed by WExplore. *Biophys. J.* **2017**, *112*, 620–629.
- (32) Lotz, S. D.; Dickson, A. Unbiased Molecular Dynamics of 11 Min Timescale Drug Unbinding Reveals Transition State Stabilizing Interactions. *J. Am. Chem. Soc.* **2018**, *140*, 618–628.
- (33) Cuzzolin, A.; Sturlese, M.; Deganutti, G.; Salmaso, V.; Sabbadin, D.; Ciancetta, A.; Moro, S. Deciphering the Complexity of Ligand-Protein Recognition Pathways Using Supervised Molecular Dynamics (SuMD) Simulations. *J. Chem. Inf. Model.* **2016**, *56*, 687–705.
- (34) Rosenbaum, D. M.; Rasmussen, S. G. F.; Kobilka, B. K. The Structure and Function of G-Protein-Coupled Receptors. *Nature* **2009**, *459*, 356–363.
- (35) Hauser, A. S.; Attwood, M. M.; Rask-Andersen, M.; Schiöth, H. B.; Gloriam, D. E. Trends in GPCR Drug Discovery: New Agents, Targets and Indications. *Nat. Rev. Drug Discov.* **2017**, *16*, 829–842.
- (36) Deganutti, G.; Moro, S.; Reynolds, C. A. Peeking at G-Protein-Coupled Receptors through the Molecular Dynamics Keyhole. *Future Med. Chem.* **2019**, *11*, 599–615.
- (37) Velgy, N.; Hedger, G.; Biggin, P. C. GPCRs: What Can We Learn from Molecular Dynamics Simulations? *Methods Mol. Biol.* **2018**, *1705*, 133–158.
- (38) Deganutti, G.; Cuzzolin, A.; Ciancetta, A.; Moro, S. Understanding Allosteric Interactions in G Protein-Coupled Receptors Using Supervised Molecular Dynamics: A Prototype Study Analysing the Human A3 Adenosine Receptor Positive Allosteric Modulator LUF6000. *Bioorg. Med. Chem.* **2015**, *23*, 4065–4071.
- (39) Deganutti, G.; Welihinda, A.; Moro, S. Comparison of the Human A2A Adenosine Receptor Recognition by Adenosine and Inosine: New Insight from Supervised Molecular Dynamics Simulations. *ChemMedChem* **2017**, *12*, 1319–1326.
- (40) Deganutti, G.; Salmaso, V.; Moro, S. Could Adenosine Recognize Its Receptors with a Stoichiometry Other than 1 : 1? *Mol. Inform.* **2018**, *37*, e1800009.
- (41) Deganutti, G.; Moro, S. Supporting the Identification of Novel Fragment-Based Positive Allosteric Modulators Using a Supervised Molecular Dynamics Approach: A Retrospective Analysis Considering the Human A2A Adenosine Receptor as a Key Example. *Molecules* **2017**, *22*.
- (42) Salmaso, V.; Sturlese, M.; Cuzzolin, A.; Moro, S. Exploring Protein-Peptide Recognition Pathways Using a Supervised Molecular Dynamics Approach. *Structure* **2017**, *25*, 655–662.e2.
- (43) Sabbadin, D.; Moro, S. Supervised Molecular Dynamics (SuMD) as a Helpful Tool to Depict GPCR-Ligand Recognition Pathway in a Nanosecond Time Scale. *J. Chem. Inf. Model.* **2014**, *54*, 372–376.
- (44) Bower, R. L.; Yule, L.; Rees, T. A.; Deganutti, G.; Hendrikse, E. R.; Harris, P. W. R.; Kowalczyk, R.; Ridgway, Z.; Wong, A. G.; Swierkula, K.; Raleigh, D. P.; Pioszak, A. A.; Brimble, M. A.; Reynolds, C. A.; Walker, C. S.; Hay, D. L. Molecular Signature for Receptor Engagement in the Metabolic Peptide Hormone Amylin. *ACS Pharmacol. Transl. Sci.* **2018**, *1*, 32–49.
- (45) Tribello, G. A.; Bonomi, M.; Branduardi, D.; Camilloni, C.; Bussi, G. PLUMED 2: New Feathers for an Old Bird. *Comput Phys Commun* **2014**, *185*, 604–613.
- (46) Huang, J.; MacKerell, A. D. CHARMM36 All-Atom Additive Protein Force Field: Validation Based on Comparison to NMR Data. *J. Comput. Chem.* **2013**, *34*, 2135–

- 2145.
- (47) Huang, J.; Rauscher, S.; Nawrocki, G.; Ran, T.; Feig, M.; de Groot, B. L.; Grubmüller, H.; MacKerell, A. D. CHARMM36m: An Improved Force Field for Folded and Intrinsically Disordered Proteins. *Nat. Methods* **2017**, *14*, 71–73.
 - (48) Vanommeslaeghe, K.; MacKerell, A. D. Automation of the CHARMM General Force Field (CGenFF) I: Bond Perception and Atom Typing. *J. Chem. Inf. Model.* **2012**, *52*, 3144–3154.
 - (49) Vanommeslaeghe, K.; Raman, E. P.; MacKerell, A. D. Automation of the CHARMM General Force Field (CGenFF) II: Assignment of Bonded Parameters and Partial Atomic Charges. *J. Chem. Inf. Model.* **2012**, *52*, 3155–3168.
 - (50) Yu, W.; He, X.; Vanommeslaeghe, K.; MacKerell, A. D. Extension of the CHARMM General Force Field to Sulfonyl-Containing Compounds and Its Utility in Biomolecular Simulations. *J. Comput. Chem.* **2012**, *33*, 2451–2468.
 - (51) Cuzzolin, A.; Deganutti, G.; Salmaso, V.; Sturlese, M.; Moro, S. AquaMMapS: An Alternative Tool to Monitor the Role of Water Molecules During Protein-Ligand Association. *ChemMedChem* **2018**, *13*, 522–531.
 - (52) Doerr, S.; Harvey, M. J.; Noé, F.; De Fabritiis, G. HTMD: High-Throughput Molecular Dynamics for Molecular Discovery. *J. Chem. Theory Comput.* **2016**, *12*, 1845–1852.
 - (53) Lebon, G.; Warne, T.; Edwards, P. C.; Bennett, K.; Langmead, C. J.; Leslie, A. G. W.; Tate, C. G. Agonist-Bound Adenosine A2A Receptor Structures Reveal Common Features of GPCR Activation. *Nature* **2011**, *474*, 521–525.
 - (54) Draper-Joyce, C. J.; Khoshouei, M.; Thal, D. M.; Liang, Y.-L.; Nguyen, A. T. N.; Furness, S. G. B.; Venugopal, H.; Baltos, J.-A.; Plitzko, J. M.; Danev, R.; Baumeister, W.; May, L. T.; Wootten, D.; Sexton, P. M.; Glukhova, A.; Christopoulos, A. Structure of the Adenosine-Bound Human Adenosine A1 Receptor-Gi Complex. *Nature* **2018**, *558*, 559–563.
 - (55) Liu, W.; Chun, E.; Thompson, A. A.; Chubukov, P.; Xu, F.; Katritch, V.; Han, G. W.; Roth, C. B.; Heitman, L. H.; IJzerman, A. P.; Cherezov, V.; Stevens, R. C. Structural Basis for Allosteric Regulation of GPCRs by Sodium Ions. *Science* **2012**, *337*, 232–236.
 - (56) Suno, R.; Kimura, K. T.; Nakane, T.; Yamashita, K.; Wang, J.; Fujiwara, T.; Yamanaka, Y.; Im, D.; Horita, S.; Tsujimoto, H.; Tawaramoto, M. S.; Hirokawa, T.; Nango, E.; Tono, K.; Kameshima, T.; Hatsui, T.; Joti, Y.; Yabashi, M.; Shimamoto, K.; Yamamoto, M.; Rosenbaum, D. M.; Iwata, S.; Shimamura, T.; Kobayashi, T. Crystal Structures of Human Orexin 2 Receptor Bound to the Subtype-Selective Antagonist EMPA. *Structure* **2018**, *26*, 7–19.e5.
 - (57) Haga, K.; Kruse, A. C.; Asada, H.; Yurugi-Kobayashi, T.; Shiroishi, M.; Zhang, C.; Weis, W. I.; Okada, T.; Kobilka, B. K.; Haga, T.; Kobayashi, T. Structure of the Human M2 Muscarinic Acetylcholine Receptor Bound to an Antagonist. *Nature* **2012**, *482*, 547–551.
 - (58) Floris, M.; Sabbadin, D.; Ciancetta, A.; Medda, R.; Cuzzolin, A.; Moro, S. Implementing the “Best Template Searching” Tool into Adenosiland Platform. *In Silico Pharmacol* **2013**, *1*, 25.
 - (59) Eswar, N.; Webb, B.; Marti-Renom, M. A.; Madhusudhan, M. S.; Eramian, D.; Shen, M.-Y.; Pieper, U.; Sali, A. Comparative Protein Structure Modeling Using Modeller. *Curr Protoc Bioinformatics* **2006**, *Chapter 5*, Unit 5.6.
 - (60) Dolinsky, T. J.; Nielsen, J. E.; McCammon, J. A.; Baker, N. A. PDB2PQR: An

- Automated Pipeline for the Setup of Poisson-Boltzmann Electrostatics Calculations. *Nucleic Acids Res.* **2004**, *32*, W665-7.
- (61) Olsson, M. H. M.; Søndergaard, C. R.; Rostkowski, M.; Jensen, J. H. PROPKA3: Consistent Treatment of Internal and Surface Residues in Empirical PK Predictions. *J. Chem. Theory Comput.* **2011**, *7*, 525–537.
- (62) Sommer, B. Membrane Packing Problems: A Short Review on Computational Membrane Modeling Methods and Tools. *Comput Struct Biotechnol J* **2013**, *5*, e201302014.
- (63) Lomize, M. A.; Lomize, A. L.; Pogozheva, I. D.; Mosberg, H. I. OPM: Orientations of Proteins in Membranes Database. *Bioinformatics* **2006**, *22*, 623–625.
- (64) Jorgensen, W. L.; Chandrasekhar, J.; Madura, J. D.; Impey, R. W.; Klein, M. L. Comparison of Simple Potential Functions for Simulating Liquid Water. *J. Chem. Phys.* **1983**, *79*, 926.
- (65) Johansson, B.; Parkinson, F. E.; Fredholm, B. B. Effects of Mono- and Divalent Ions on the Binding of the Adenosine Analogue CGS 21680 to Adenosine A2 Receptors in Rat Striatum. *Biochem. Pharmacol.* **1992**, *44*, 2365–2370.
- (66) Gutiérrez-de-Terán, H.; Massink, A.; Rodríguez, D.; Liu, W.; Han, G. W.; Joseph, J. S.; Katritch, I.; Heitman, L. H.; Xia, L.; Ijzerman, A. P.; Cherezov, V.; Katritch, V.; Stevens, R. C. The Role of a Sodium Ion Binding Site in the Allosteric Modulation of the A(2A) Adenosine G Protein-Coupled Receptor. *Structure* **2013**, *21*, 2175–2185.
- (67) Harvey, M. J.; Giupponi, G.; Fabritiis, G. D. ACEMD: Accelerating Biomolecular Dynamics in the Microsecond Time Scale. *J. Chem. Theory Comput.* **2009**, *5*, 1632–1639.
- (68) Berendsen, H. J. C.; Postma, J. P. M.; van Gunsteren, W. F.; DiNola, A.; Haak, J. R. Molecular Dynamics with Coupling to an External Bath. *J. Chem. Phys.* **1984**, *81*, 3684.
- (69) Loncharich, R. J.; Brooks, B. R.; Pastor, R. W. Langevin Dynamics of Peptides: The Frictional Dependence of Isomerization Rates of N-Acetylalanyl-N'-Methylamide. *Biopolymers* **1992**, *32*, 523–535.
- (70) Forester, T. R.; Smith, W. SHAKE, Rattle, and Roll: Efficient Constraint Algorithms for Linked Rigid Bodies. *J. Comput. Chem.* **1998**.
- (71) Kräutler, V.; van Gunsteren, W. F.; Hünenberger, P. H. A Fast SHAKE Algorithm to Solve Distance Constraint Equations for Small Molecules in Molecular Dynamics Simulations. *J. Comput. Chem.* **2001**, *22*, 501–508.
- (72) Essmann, U.; Perera, L.; Berkowitz, M. L.; Darden, T.; Lee, H.; Pedersen, L. G. A Smooth Particle Mesh Ewald Method. *J. Chem. Phys.* **1995**, *103*, 8577.
- (73) Saleh, N.; Ibrahim, P.; Saladino, G.; Gervasio, F. L.; Clark, T. An Efficient Metadynamics-Based Protocol To Model the Binding Affinity and the Transition State Ensemble of G-Protein-Coupled Receptor Ligands. *J. Chem. Inf. Model.* **2017**, *57*, 1210–1217.
- (74) Humphrey, W.; Dalke, A.; Schulten, K. VMD: Visual Molecular Dynamics. *J Mol Graph* **1996**, *14*, 33–38, 27.
- (75) Miller, B. R.; McGee, T. D.; Swails, J. M.; Homeyer, N.; Gohlke, H.; Roitberg, A. E. MMPBSA.py: An Efficient Program for End-State Free Energy Calculations. *J. Chem. Theory Comput.* **2012**, *8*, 3314–3321.
- (76) Ballesteros, J. A.; Weinstein, H. [19] Integrated Methods for the Construction of Three-Dimensional Models and Computational Probing of Structure-Function Relations in G

- Protein-Coupled Receptors. In *Receptor Molecular Biology*; Methods in Neurosciences; Elsevier, 1995; Vol. 25, pp. 366–428.
- (77) Jacobson, K. A. Introduction to Adenosine Receptors as Therapeutic Targets. *Handb Exp Pharmacol* **2009**, 1–24.
- (78) Chen, J.-F.; Eltzschig, H. K.; Fredholm, B. B. Adenosine Receptors as Drug Targets--What Are the Challenges? *Nat. Rev. Drug Discov.* **2013**, *12*, 265–286.
- (79) Jacobson, K. A.; Gao, Z.-G. Adenosine Receptors as Therapeutic Targets. *Nat. Rev. Drug Discov.* **2006**, *5*, 247–264.
- (80) Pardoll, D. M. The Blockade of Immune Checkpoints in Cancer Immunotherapy. *Nat. Rev. Cancer* **2012**, *12*, 252–264.
- (81) Isberg, V.; Mordalski, S.; Munk, C.; Rataj, K.; Harpsøe, K.; Hauser, A. S.; Vroling, B.; Bojarski, A. J.; Vriend, G.; Gloriam, D. E. GPCRdb: An Information System for G Protein-Coupled Receptors. *Nucleic Acids Res.* **2016**, *44*, D356–64.
- (82) Carpenter, B.; Nehmé, R.; Warne, T.; Leslie, A. G. W.; Tate, C. G. Structure of the Adenosine A_{2A} Receptor Bound to an Engineered G Protein. *Nature* **2016**, *536*, 104–107.
- (83) Lee, Y.; Kim, S.; Choi, S.; Hyeon, C. Ultraslow Water-Mediated Transmembrane Interactions Regulate the Activation of A_{2A} Adenosine Receptor. *Biophys. J.* **2016**, *111*, 1180–1191.
- (84) Goadsby, P. J.; Hoskin, K. L.; Storer, R. J.; Edvinsson, L.; Connor, H. E. Adenosine A₁ Receptor Agonists Inhibit Trigeminovascular Nociceptive Transmission. *Brain* **2002**, *125*, 1392–1401.
- (85) Tate, C. G.; García-Nafria, J.; Lee, Y.; Bai, X.; Carpenter, B. Cryo-EM Structure of the Adenosine A_{2A} Receptor Coupled to an Engineered Heterotrimeric G Protein. *BioRxiv* **2018**.
- (86) Cheng, R. K. Y.; Segala, E.; Robertson, N.; Deflorian, F.; Doré, A. S.; Errey, J. C.; Fiez-Vandal, C.; Marshall, F. H.; Cooke, R. M. Structures of Human A₁ and A_{2A} Adenosine Receptors with Xanthines Reveal Determinants of Selectivity. *Structure* **2017**, *25*, 1275–1285.e4.
- (87) Bhatt, D.; Zuckerman, D. M. Beyond Microscopic Reversibility: Are Observable Non-Equilibrium Processes Precisely Reversible? *J. Chem. Theory Comput.* **2011**, *7*, 2520–2527.
- (88) Dinner, A. R.; Karplus, M. Is Protein Unfolding the Reverse of Protein Folding? A Lattice Simulation Analysis. *J. Mol. Biol.* **1999**, *292*, 403–419.
- (89) Borea, P. A.; Dalpiaz, A.; Varani, K.; Gessi, S.; Gilli, G. Binding Thermodynamics at A₁ and A_{2A} Adenosine Receptors. *Life Sci.* **1996**, *59*, 1373–1388.
- (90) Schmidtke, P.; Luque, F. J.; Murray, J. B.; Barril, X. Shielded Hydrogen Bonds as Structural Determinants of Binding Kinetics: Application in Drug Design. *J. Am. Chem. Soc.* **2011**, *133*, 18903–18910.
- (91) Jiang, Q.; Van Rhee, A. M.; Kim, J.; Yehle, S.; Wess, J.; Jacobson, K. A. Hydrophilic Side Chains in the Third and Seventh Transmembrane Helical Domains of Human A_{2A} Adenosine Receptors Are Required for Ligand Recognition. *Mol. Pharmacol.* **1996**, *50*, 512–521.
- (92) Zhukov, A.; Andrews, S. P.; Errey, J. C.; Robertson, N.; Tehan, B.; Mason, J. S.; Marshall, F. H.; Weir, M.; Congreve, M. Biophysical Mapping of the Adenosine A_{2A} Receptor. *J. Med. Chem.* **2011**, *54*, 4312–4323.

- (93) Doré, A. S.; Robertson, N.; Errey, J. C.; Ng, I.; Hollenstein, K.; Tehan, B.; Hurrell, E.; Bennett, K.; Congreve, M.; Magnani, F.; Tate, C. G.; Weir, M.; Marshall, F. H. Structure of the Adenosine A(2A) Receptor in Complex with ZM241385 and the Xanthines XAC and Caffeine. *Structure* **2011**, *19*, 1283–1293.
- (94) Segala, E.; Guo, D.; Cheng, R. K. Y.; Bortolato, A.; Deflorian, F.; Doré, A. S.; Errey, J. C.; Heitman, L. H.; IJzerman, A. P.; Marshall, F. H.; Cooke, R. M. Controlling the Dissociation of Ligands from the Adenosine A2A Receptor through Modulation of Salt Bridge Strength. *J. Med. Chem.* **2016**, *59*, 6470–6479.
- (95) Gotter, A. L.; Roecker, A. J.; Hargreaves, R.; Coleman, P. J.; Winrow, C. J.; Renger, J. J. Orexin Receptors as Therapeutic Drug Targets. *Prog. Brain Res.* **2012**, *198*, 163–188.
- (96) Tiwary, P.; Limongelli, V.; Salvalaglio, M.; Parrinello, M. Kinetics of Protein-Ligand Unbinding: Predicting Pathways, Rates, and Rate-Limiting Steps. *Proc. Natl. Acad. Sci. USA* **2015**, *112*, E386-91.
- (97) Langmead, C. J.; Watson, J.; Reavill, C. Muscarinic Acetylcholine Receptors as CNS Drug Targets. *Pharmacol. Ther.* **2008**, *117*, 232–243.
- (98) Heitz, F.; Holzwarth, J. A.; Gies, J. P.; Pruss, R. M.; Trumpp-Kallmeyer, S.; Hibert, M. F.; Guenet, C. Site-Directed Mutagenesis of the Putative Human Muscarinic M2 Receptor Binding Site. *Eur. J. Pharmacol.* **1999**, *380*, 183–195.
- (99) Kruse, A. C.; Hu, J.; Pan, A. C.; Arlow, D. H.; Rosenbaum, D. M.; Rosemond, E.; Green, H. F.; Liu, T.; Chae, P. S.; Dror, R. O.; Shaw, D. E.; Weis, W. I.; Wess, J.; Kobilka, B. K. Structure and Dynamics of the M3 Muscarinic Acetylcholine Receptor. *Nature* **2012**, *482*, 552–556.
- (100) Kruse, A. C.; Ring, A. M.; Manglik, A.; Hu, J.; Hu, K.; Eitel, K.; Hübner, H.; Pardon, E.; Valant, C.; Sexton, P. M.; Christopoulos, A.; Felder, C. C.; Gmeiner, P.; Steyaert, J.; Weis, W. I.; Garcia, K. C.; Wess, J.; Kobilka, B. K. Activation and Allosteric Modulation of a Muscarinic Acetylcholine Receptor. *Nature* **2013**, *504*, 101–106.
- (101) Dror, R. O.; Green, H. F.; Valant, C.; Borhani, D. W.; Valcourt, J. R.; Pan, A. C.; Arlow, D. H.; Canals, M.; Lane, J. R.; Rahmani, R.; Baell, J. B.; Sexton, P. M.; Christopoulos, A.; Shaw, D. E. Structural Basis for Modulation of a G-Protein-Coupled Receptor by Allosteric Drugs. *Nature* **2013**, *503*, 295–299.
- (102) Hollingsworth, S. A.; Kelly, B.; Valant, C.; Michaelis, J. A.; Mastromihalis, O.; Thompson, G.; Venkatakrisnan, A. J.; Hertig, S.; Scammells, P. J.; Sexton, P. M.; Felder, C. C.; Christopoulos, A.; Dror, R. O. Cryptic Pocket Formation Underlies Allosteric Modulator Selectivity at Muscarinic GPCRs. *Nat. Commun.* **2019**, *10*, 3289.
- (103) Yu, Z.; Xu, F.; Huse, L. M.; Morisseau, C.; Draper, A. J.; Newman, J. W.; Parker, C.; Graham, L.; Engler, M. M.; Hammock, B. D.; Zeldin, D. C.; Kroetz, D. L. Soluble Epoxide Hydrolase Regulates Hydrolysis of Vasoactive Epoxyeicosatrienoic Acids. *Circ. Res.* **2000**, *87*, 992–998.
- (104) Node, K.; Huo, Y.; Ruan, X.; Yang, B.; Spiecker, M.; Ley, K.; Zeldin, D. C.; Liao, J. K. Anti-Inflammatory Properties of Cytochrome P450 Epoxygenase-Derived Eicosanoids. *Science* **1999**, *285*, 1276–1279.
- (105) Schmelzer, K. R.; Kubala, L.; Newman, J. W.; Kim, I.-H.; Eiserich, J. P.; Hammock, B. D. Soluble Epoxide Hydrolase Is a Therapeutic Target for Acute Inflammation. *Proc. Natl. Acad. Sci. USA* **2005**, *102*, 9772–9777.
- (106) Shen, H. C.; Hammock, B. D. Discovery of Inhibitors of Soluble Epoxide Hydrolase: A Target with Multiple Potential Therapeutic Indications. *J. Med. Chem.* **2012**, *55*, 1789–

- 1808.
- (107) Alexander, S. P. H.; Mathie, A.; Peters, J. A. Guide to Receptors and Channels (GRAC), 5th Edition. *Br. J. Pharmacol.* **2011**, *164 Suppl 1*, S1-324.
 - (108) Mollica, L.; Theret, I.; Antoine, M.; Perron-Sierra, F.; Charton, Y.; Fourquez, J.-M.; Wierzbicki, M.; Boutin, J. A.; Ferry, G.; Decherchi, S.; Bottegoni, G.; Ducrot, P.; Cavalli, A. Molecular Dynamics Simulations and Kinetic Measurements to Estimate and Predict Protein-Ligand Residence Times. *J. Med. Chem.* **2016**, *59*, 7167–7176.
 - (109) Bešker, N.; Gervasio, F. L. Using Metadynamics and Path Collective Variables to Study Ligand Binding and Induced Conformational Transitions. *Methods Mol. Biol.* **2012**, *819*, 501–513.
 - (110) Bernetti, M.; Masetti, M.; Recanatini, M.; Amaro, R. E.; Cavalli, A. An Integrated Markov State Model and Path Metadynamics Approach to Characterize Drug Binding Processes. *J. Chem. Theory Comput.* **2019**, *15*, 5689–5702.